J Eng Math (2017) 105:117–135
DOI 10.1007/s10665-016-9886-2

Generalized analytical solution to wave interaction with submerged multi-layer horizontal porous plate breakwaters

Zhichao Fang · Longfei Xiao · Tao Peng

Received: 7 January 2016 / Accepted: 20 October 2016 / Published online: 7 December 2016

Abstract A generalized analytical solution to wave interaction with multi-layer submerged horizontal porous plate breakwaters has been derived in the context of linear potential theory. A two-dimensional problem with N horizontal porous plate layers in a finite water depth has been formulated, and the viscous effects of the porous plates are considered using Darcy's law. In solving the spatial velocity potentials using the matched eigenfunction expansion method, techniques based on artificial potential splitting are employed to avoid complex dispersion relations. The developed analytical solution is verified by comparison with results of previous research on single- and double-layer cases and validated with the results of physical model tests. The analytical solution gives scientific insights into wave interaction with the breakwater and provides an effective and practical tool for designing its parameters. The velocity fields are computed and the way the horizontal porous plates play their role in attenuating fluid motion is illustrated. The effects of various parameters (i.e., plate submergence, width, porosity, layer number, and wave parameter) on the overall hydrodynamic and wave dissipation performance are discussed. The results indicate that a breakwater with multi-layer horizontal porous plates exhibits improved performance.

Keywords Analytical solution · Energy dissipation · Horizontal porous plate · Matched eigenfunction expansion method · Transmission coefficient

1 Introduction

Submerged breakwaters with horizontal porous plates have proved efficient at dissipating wave energy and thus protecting coastlines and harbour structures [1]. Compared with a solid plate, a porous plate can significantly reduce the wave forces acting or even impacting on it. Additionally, horizontal plate breakwaters are less dependent on the geological condition of the local seabed and relatively insensitive to the water depth, thus being economical in

Z. Fang · L. Xiao (✉) · T. Peng
State Key Laboratory of Ocean Engineering, Shanghai Jiao Tong University, Shanghai 200240, China
e-mail: xiaolf@sjtu.edu.cn

Z. Fang
e-mail: zhichaofang@sjtu.org

T. Peng
e-mail: pengtao@sjtu.edu.cn

practice. Because of these advantages, the hydrodynamic performance of horizontal porous plate breakwaters has aroused considerable interest among researchers and designers in this field.

Research on the performance of horizontal porous plates began with the studies by Yu and Chwang [2] on wave interaction with a submerged porous plate using the boundary element method (BEM). The boundary condition of a porous plate was proposed based on the assumption that the flow passing through a porous medium satisfied Darcy's law [3,4] (i.e., a linear relation between the normal seepage velocity and the corresponding pressure difference). Related studies undertaken using the matched eigenfunction expansion method on different porous plate structures were performed by Chwang and Wu [5] and Yu [6]. Darcy's law describes the characteristic of water flow passing through a porous medium in a linearized formula and has been applied in a large number of studies of water wave interaction with porous structures (see [7]). Also, many researchers have investigated wave interaction with various types of horizontal plate breakwaters and the performance of combined structures of a horizontal plate and a vertical wall based on the linear potential theory. Numerical methods, such as the BEM, were applied in some of these studies (e.g., [8–10]); however, the matched eigenfunction expansion method has been used more frequently (e.g., [9–18]). The monochromatic incident wave interaction with a horizontal porous flexible plate was investigated by Cho and Kim [9] and Behera and Sahoo [18], and the hydrodynamic characteristics of a vertical porous flexible barrier (bottom-touching or surface-piercing) near the end of a semi-infinitely long channel of finite water depth was discussed by Yip et al. [14]. The flexibility and motion-induced waves may have significant effect on the wave-dissipating performance of the plate. In [9], the results derived by the matched eigenfunction expansion method were verified by those obtained by the multi-domain BEM and also validated by a series of experiments. The performance of inclined perforated plates was studied and discussed by Cho and Kim [10], and the results showed that a proper inclination angle of the plate positioned near to the free surface could improve its wave-absorbing efficiency. Liu et al. [15] derived an analytical solution for a modified Jarlan-type breakwater with an internal submerged horizontal porous plate, and the results suggested that the breakwater could achieve satisfactory performance with the appropriate geometric porosity of both the vertical and the horizontal plates. Liu et al. [16] examined the hydrodynamic performance of a breakwater with two layers of submerged horizontal plates, in which the upper plate was permeable while the lower plate was solid, and the results suggested that the breakwater might experience enhanced performance if the lower plate were also perforated. Furthermore, a quadratic relation between the traversing velocity and the pressure loss was considered in [19,20], and the situation of wave scattering by a submerged plate with finite thickness was investigated in [21,22].

When constructing the eigenfunction expansions in the cases of breakwaters with horizontal porous plates, the conventional method combines the boundary conditions on the free surface, the rigid seabed and the porous plate(s) to form the complex dispersion relations which are complete over the whole depth in order to obtain the eigenvalues (e.g., [5,9,12,15]). Because the complex dispersion relation is too complicated to be formulated mathematically in the multi-layer case, the standard matched eigenfunction expansion method can hardly be applied directly to multi-layer horizontal porous-plate breakwaters. In order to overcome this limitation, Liu and Li [23] proposed an alternative analytical solution without complex wave dispersion relations by introducing artificial potentials. Based on this methodology, Cho et al. [24] derived an analytical solution to a breakwater with double-layer submerged horizontal porous plates, which was verified through results obtained from both BEM and experiments. In addition, some further verifications and discussions of this analytical solution can also be found in [25].

All of the solutions cited above only considered the problems of single- or double-layer horizontal porous plates. For solid plates, Wang and Shen [26] analytically investigated the case of wave reflection and transmission over a group of submerged horizontal solid plates. In the case of perforated wall breakwaters, Liu et al. [27] developed an analytical solution to multi-chamber perforated caissons, and indicated that double- or three-chamber caissons are favorable to wave absorbing performance. However, few research papers have referred to breakwaters with multi-layer of horizontal porous plates.

The present paper is concerned with the feasibility and efficiency of a breakwater with multi-layer submerged horizontal porous plates. A generalized analytical solution, which is expected to give scientific insights into the problem and to serve as an effective tool for breakwater design, has been derived by means of the two-dimensional linearized potential theory and the matched eigenfunction expansion method. The present solution was verified

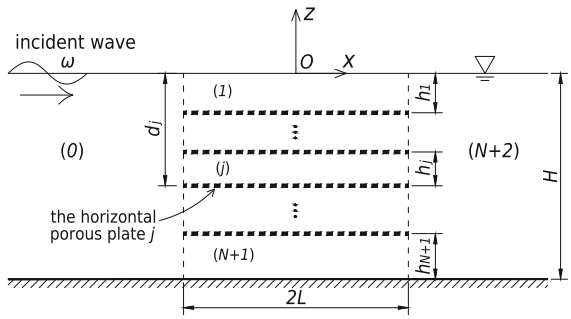

Fig. 1 Sketch of a two-dimensional model of a breakwater with N layers of submerged horizontal porous plates

through comparisons with previous results and validated against physical model tests. Subsequently, taking a three-layer breakwater as an example, the velocity fields were computed, and the effects of different parameters of horizontal plates on the hydrodynamic performance of the breakwater were examined. Additionally, a simple procedure for its optimization design based on reducing the wave transmission coefficient was discussed.

2 Analytical solutions

2.1 Mathematical formulation

Considering the interaction of monochromatic normally incident waves with stationary submerged porous horizontal plates, the problem can be idealized in two dimensions. A sketch of Cartesian coordinate system of a submerged multi-layer horizontal porous-plate breakwater is given in Fig. 1. There are in total N layers of porous plates located in water of constant depth H. The width of the plates is $2L$, and the thickness of each is assumed to be zero owing to its relatively small value in comparison with the incident wavelength and the water depth. The submerged depth of plate j is d_j, and the spacing between plates $j-1$ and j is $h_j = d_j - d_{j-1}$ ($j \geq 2$). In particular, $h_1 = d_1$ and $d_{N+1} = H$. All these plates of N layers divide the entire fluid domain into $N+3$ subregions, as numbered in Fig. 1.

Assuming that the fluid is inviscid and incompressible and the flow is irrotational, a velocity potential $\Phi(x, z, t)$ can be used to describe the fluid motion, where t is time. Considering a linear incident wave of frequency ω, the velocity potential can be written as $\Phi(x, z, t) = \mathfrak{Re}\left[\phi(x, z)\mathrm{e}^{-\mathrm{i}\omega t}\right]$, thereby separating the spatial part from Φ, where $\mathfrak{Re}[\,]$ denotes the real part of the argument, ϕ denotes the spatial velocity potential, and $\mathrm{i} = \sqrt{-1}$. The spatial velocity potential ϕ_j in the subregion j satisfies the Laplace equation:

$$\frac{\partial^2 \phi_j}{\partial x^2} + \frac{\partial^2 \phi_j}{\partial z^2} = 0, \quad j = 0, 1, \ldots, N+2, \tag{1}$$

and relevant boundary conditions on the free surface, seabed, far field, and at the plate tips, which are written, respectively, as:

$$\frac{\partial \phi_j}{\partial z} = \frac{\omega^2}{g}\phi_j, \quad z = 0,\ j = 0, 1, N+2, \tag{2}$$

$$\frac{\partial \phi_j}{\partial z} = 0, \quad z = -H,\ j = 0, N+1, N+2, \tag{3}$$

$$\lim_{x \to -\infty} \left(\frac{\partial}{\partial x} + \mathrm{i}k\right) \phi_{\mathrm{R}} = 0, \tag{4}$$

$$\lim_{x \to +\infty} \left(\frac{\partial}{\partial x} - \mathrm{i}k\right) \phi_{N+2} = 0, \tag{5}$$

$$|\nabla \phi| = \mathcal{O}(r^{\pm -1/2}) \quad \text{as } r^{\pm} = \left((x \mp L)^2 + \left(z + d_j\right)^2\right)^{1/2} \to 0, \quad j = 1, 2, \ldots, N, \tag{6}$$

where g denotes the gravitational acceleration, k denotes the incident wave number, and ϕ_R represents the reflected velocity potential. Equation (6) represents the square-root type singularity in the velocity field at the plate tips (see [28, p. 40]).

In addition, the matching conditions between different subregions must also be satisfied:

$$\frac{\partial \phi_j}{\partial z} = \frac{\partial \phi_{j+1}}{\partial z} = \mathrm{i}kG_j\left(\phi_{j+1} - \phi_j\right), \quad z = -d_j,\ j = 1, 2, \ldots, N, \tag{7}$$

$$\phi_0 = \phi_j, \quad x = -L,\ j = 1, 2, \ldots, N+1, \tag{8}$$

$$\frac{\partial \phi_0}{\partial x} = \frac{\partial \phi_j}{\partial x}, \quad x = -L,\ j = 1, 2, \ldots, N+1, \tag{9}$$

$$\phi_{N+2} = \phi_j, \quad x = L,\ j = 1, 2, \ldots, N+1, \tag{10}$$

$$\frac{\partial \phi_{N+2}}{\partial x} = \frac{\partial \phi_j}{\partial x}, \quad x = L,\ j = 1, 2, \ldots, N+1. \tag{11}$$

Equation (7) is the porous boundary condition for a thin, but rigid permeable plate based on the assumption that the plate is made of material with very fine pores. The complex number G_j ($j = 1, 2, \ldots, N$) is the dimensionless porous effect parameter of each horizontal porous plate, depending on the porosity, linearized resistance coefficient, and added mass coefficient (see [6,29]). The real part of G_j relates to the resistance of the porous plate against the seepage flow, while the imaginary part denotes the inertial effect (or phase-shift effect) (see [9,30,31]). When the plate is solid or the resistance coefficient tends to be infinity, $G_j = 0$. A larger $|G_j|$ means that the plate is more transparent. In the present study, G_j is considered as a real number because the phase lag of G_j is negligibly small for a thin porous plate with small to moderate porosity (see [1,9]), and then the porous plate boundary condition is reduced to Darcy's law, which was applied in [2,4,5].

It is noted that the matching conditions on $x = \pm L$ (i.e., (8)–(11)) represent, physically, the continuity of the fluid pressure and mass flux. Mathematically, these conditions imply that the potentials ϕ_0 and ϕ_{N+2} are the harmonic continuations of ϕ_j ($j = 1,\ 2,\ \ldots,\ N$) (see [32, Chapter X, §5, Theorem VI]).

2.2 Decomposition of velocity potentials

Because of the symmetry of the fluid domain and the breakwater structure, ϕ can be split into a symmetric part (ϕ^{S}) and an anti-symmetric part (ϕ^{A}):

$$\phi = \frac{1}{2}\left(\phi^{\mathrm{S}} + \phi^{\mathrm{A}}\right), \tag{12}$$

$$\phi^{\mathrm{S}}(-x, z) = \phi^{\mathrm{S}}(x, z), \tag{13}$$

$$\phi^{\mathrm{A}}(-x, z) = -\phi^{\mathrm{A}}(x, z). \tag{14}$$

Thus, only the left half region $x < 0$ needs to be taken into consideration when solving this problem.

The major difficulty in solving the boundary value problem (Eqs. (1)–(11)) refers to the non-homogeneous porous plate boundary condition (see Eq. (7)). The normal velocities through the plates are initially unknown, and complex dispersion equations need to be solved in the conventional solution. The present approach linearly decomposes the potentials inside the breakwater into two parts, one with *vertically* homogeneous boundary conditions and the other with *horizontally* homogeneous boundary conditions: $\phi_j^{\mathrm{S}} = \phi_{j,v}^{\mathrm{S}} + \phi_{j,h}^{\mathrm{S}}$ and $\phi_j^{\mathrm{A}} = \phi_{j,v}^{\mathrm{A}} + \phi_{j,h}^{\mathrm{A}}$ ($j = 1, 2, \ldots, N+1$). This technique was first advanced by Lee [33], and then was employed in [23,24,34]. The horizontal expansions $\phi_{j,h}^{\mathrm{S}}$ and $\phi_{j,h}^{\mathrm{A}}$, which are constructed using either homogeneous Dirichlet or Neumann conditions on $x = -L$ and $x = 0$, are the particular solutions that account for the normal velocities on the plates. In each subregion, because the horizontal expansions are subtracted from the full solution, the remainder must satisfy the homogeneous Neumann conditions on the plates. These conditions are then the basis of the vertical expansions $\phi_{j,v}^{\mathrm{S}}$ and $\phi_{j,v}^{\mathrm{A}}$. Therefore, the boundary conditions can be rewritten as follows:

$$\frac{\partial \phi_0^{\mathrm{S(A)}}}{\partial z} = \frac{\omega^2}{g}\phi_0^{\mathrm{S(A)}}, \quad z = 0, \tag{15}$$

$$\frac{\partial \phi_0^{\mathrm{S(A)}}}{\partial z} = 0, \quad z = -H, \tag{16}$$

$$\lim_{x\to-\infty}\left(\frac{\partial}{\partial x} + \mathrm{i}k\right)\phi_{\mathrm{R}}^{\mathrm{S(A)}} = 0, \tag{17}$$

$$\frac{\partial \phi_{1,v}^{\mathrm{S(A)}}}{\partial z} = \frac{\omega^2}{g}\phi_{1,v}^{\mathrm{S(A)}}, \quad z = 0, \tag{18}$$

$$\frac{\partial \phi_{j,v}^{\mathrm{S(A)}}}{\partial z} = 0, \quad z = -d_j,\ j = 1, 2, \ldots, N+1, \tag{19}$$

$$\frac{\partial \phi_{j,v}^{\mathrm{S(A)}}}{\partial z} = 0, \quad z = -d_{j-1},\ j = 2, 3, \ldots, N+1, \tag{20}$$

$$\frac{\partial \phi_{j,v}^{\mathrm{S}}}{\partial x} = 0,\ \phi_{j,v}^{\mathrm{A}} = 0, \quad x = 0,\ j = 1, 2, \ldots, N+1, \tag{21}$$

$$\frac{\partial \phi_{1,h}^{\mathrm{S(A)}}}{\partial z} = \frac{\omega^2}{g}\phi_{1,h}^{\mathrm{S(A)}}, \quad z = 0, \tag{22}$$

$$\frac{\partial \phi_{N+1,h}^{\mathrm{S(A)}}}{\partial z} = 0, \quad z = -H, \tag{23}$$

$$\phi_{j,h}^{\mathrm{S}} = 0,\ \frac{\partial \phi_{j,h}^{\mathrm{A}}}{\partial x} = 0, \quad x = -L,\ j = 1, 2, \ldots, N+1, \tag{24}$$

$$\frac{\partial \phi_{j,h}^{\mathrm{S}}}{\partial x} = 0,\ \phi_{j,h}^{\mathrm{A}} = 0, \quad x = 0,\ j = 1, 2, \ldots, N+1, \tag{25}$$

and the matching conditions:

$$\frac{\partial \phi_{j,h}^{\mathrm{S(A)}}}{\partial z} = \frac{\partial \phi_{j+1,h}^{\mathrm{S(A)}}}{\partial z} = \mathrm{i}kG_j\left(\phi_{j+1}^{\mathrm{S(A)}} - \phi_j^{\mathrm{S(A)}}\right), \quad z = -d_j,\ j = 1, 2, \ldots, N, \tag{26}$$

$$\phi_0^{\mathrm{S}} = \phi_{j,v}^{\mathrm{S}},\ \phi_0^{\mathrm{S}} = \phi_{j,v}^{\mathrm{A}} + \phi_{j,h}^{\mathrm{A}}, \quad x = -L,\ j = 1, 2, \ldots, N+1, \tag{27}$$

$$\frac{\partial \phi_0^{\mathrm{S}}}{\partial x} = \frac{\partial \phi_{j,v}^{\mathrm{S}}}{\partial x} + \frac{\partial \phi_{j,h}^{\mathrm{S}}}{\partial x},\ \frac{\partial \phi_0^{\mathrm{A}}}{\partial x} = \frac{\partial \phi_{j,v}^{\mathrm{A}}}{\partial x}, \quad x = -L,\ j = 1, 2, \ldots, N+1. \tag{28}$$

Accordingly, the eigenfunction expansion form of potentials in each subregion along with the eigenvalues can be obtained without solving any complex dispersion equation, thus parrying the considerable difficulty in solving the complex dispersion equations. Thereafter, applying the non-homogeneous matching conditions, i.e., the porous plate conditions on $z = -d_j$ (Eq. (26)) and the flex and pressure continuity conditions on $x = -L$ (Eqs. (27) and (28), respectively), the unknown coefficients in the eigenfunction expansions can be determined. Because of the linearity of both the Laplace equation and the boundary conditions, the problem written as $\phi_0 = (\phi_0^{\mathrm{S}} + \phi_0^{\mathrm{A}})/2$ and $\phi_j = (\phi_{j,v}^{\mathrm{S}} + \phi_{j,h}^{\mathrm{S}} + \phi_{j,v}^{\mathrm{A}} + \phi_{j,h}^{\mathrm{A}})/2$ $(j = 1, 2, \ldots, N+1)$ is equivalent to the original system (1)–(11) and, therefore, yields the same solution.

2.3 Matched eigenfunction expansion method

By the method of separation of variables according to the boundary conditions in Eqs. (15)–(25), the velocity potentials in eigenfunction expansion form can be obtained. In constructing the expansions in Eqs. (31) and (35), the first equality in Eq. (7), which represents the continuity of mass flux at the horizontal plates, has been satisfied.

The symmetrical and anti-symmetrical potentials in the subregion $N+2$ are obtained based on the potentials in the subregion 0 according to Eqs. (13) and (14), respectively. The symmetrical velocity potential in each subregion can be written as:

$$\phi_0^{\mathrm{S}} = -\frac{\mathrm{i}g\zeta_0}{2\omega}\left[\left(\mathrm{e}^{k_0(x+L)} + a_0\mathrm{e}^{-k_0(x+L)}\right)Z_0(z) + \sum_{m=1}^{\infty} a_m \mathrm{e}^{k_m(x+L)} Z_m(z)\right], \tag{29}$$

$$\phi_{j,v}^{\mathrm{S}} = \begin{cases} -\dfrac{\mathrm{i}g\zeta_0}{2\omega}\left[\displaystyle\sum_{m=0}^{\infty} b_m^1 \frac{\cosh(\lambda_m x)}{\cosh(\lambda_m L)} f_{1,m}(z)\right], & j=1, \\ -\dfrac{\mathrm{i}g\zeta_0}{2\omega}\left[b_0^j + \displaystyle\sum_{m=1}^{\infty} b_m^j \frac{\cosh\left(\kappa_m^j x\right)}{\cosh\left(\kappa_m^j L\right)} f_{j,m}(z)\right], & j=2,3,\ldots,N+1, \end{cases} \tag{30}$$

$$\phi_{j,h}^{\mathrm{S}} = \begin{cases} -\dfrac{\mathrm{i}g\zeta_0}{2\omega}\left\{\displaystyle\sum_{m'=0}^{\infty} \frac{1}{\mu_{m'}} c_{m'}^1 g_{m'}(x)\left[\eta_{m'}\cosh\mu_{m'}(z+d_1) + \sinh\mu_{m'}(z+d_1)\right]\right\}, & j=1, \\ -\dfrac{\mathrm{i}g\zeta_0}{2\omega}\left[\displaystyle\sum_{m'=0}^{\infty} g_{m'}(x)\frac{c_{m'}^{j-1}\cosh\mu_{m'}(z+d_j) - c_{m'}^j\cosh\mu_{m'}(z+d_{j-1})}{\mu_{m'}\sinh(\mu_{m'}h_j)}\right], & j=2,3,\ldots,N, \\ -\dfrac{\mathrm{i}g\zeta_0}{2\omega}\left[\displaystyle\sum_{m'=0}^{\infty} g_{m'}(x)\frac{c_{m'}^N\cosh\mu_{m'}(z+H)}{\mu_{m'}\sinh(\mu_{m'}h_{N+1})}\right], & j=N+1, \end{cases} \tag{31}$$

$$\phi_{N+2}^{\mathrm{S}} = \phi_0^{\mathrm{S}}(-x,z), \tag{32}$$

and the anti-symmetrical parts can be written as:

$$\phi_0^{\mathrm{A}} = -\frac{\mathrm{i}g\zeta_0}{2\omega}\left[\left(\mathrm{e}^{k_0(x+L)} + \bar{a}_0\mathrm{e}^{-k_0(x+L)}\right)Z_0(z) + \sum_{m=1}^{\infty} \bar{a}_m \mathrm{e}^{k_m(x+L)} Z_m(z)\right], \tag{33}$$

$$\phi_{j,v}^{\mathrm{A}} = \begin{cases} -\dfrac{\mathrm{i}g\zeta_0}{2\omega}\left[-\displaystyle\sum_{m=0}^{\infty} \bar{b}_m^1 \frac{\sinh(\lambda_m x)}{\sinh(\lambda_m L)} f_{1,m}(z)\right], & j=1, \\ -\dfrac{\mathrm{i}g\zeta_0}{2\omega}\left[-\bar{b}_0^j\dfrac{x}{L} - \displaystyle\sum_{m=1}^{\infty} \bar{b}_m^j \frac{\sinh(\kappa_m^j x)}{\sinh(\kappa_m^j L)} f_{j,m}(z)\right], & j=2,3,\ldots,N+1, \end{cases} \tag{34}$$

$$\phi_{j,h}^{\mathrm{A}} = \begin{cases} -\dfrac{\mathrm{i}g\zeta_0}{2\omega}\left\{\displaystyle\sum_{m'=0}^{\infty} \frac{1}{\mu_{m'}} \bar{c}_{m'}^1 \bar{g}_{m'}(x)\left[\eta_{m'}\cosh\mu_{m'}(z+d_1) + \sinh\mu_{m'}(z+d_1)\right]\right\}, & j=1, \\ -\dfrac{\mathrm{i}g\zeta_0}{2\omega}\left[\displaystyle\sum_{m'=0}^{\infty} \bar{g}_{m'}(x)\frac{\bar{c}_{m'}^{j-1}\cosh\mu_{m'}(z+d_j) - \bar{c}_{m'}^j\cosh\mu_{m'}(z+d_{j-1})}{\mu_{m'}\sinh(\mu_{m'}h_j)}\right], & j=2,3,\ldots,N, \\ -\dfrac{\mathrm{i}g\zeta_0}{2\omega}\left[\displaystyle\sum_{m'=0}^{\infty} \bar{g}_{m'}(x)\frac{\bar{c}_m^N\cosh\mu_{m'}(z+H)}{\mu_{m'}\sinh(\mu_{m'}h_{N+1})}\right], & j=N+1, \end{cases} \tag{35}$$

$$\phi_{N+2}^{\mathrm{A}} = -\phi_0^{\mathrm{A}}(-x,z), \tag{36}$$

where ζ_0 is the incident wave height,

$$\eta_{m'} = \frac{\omega^2\tanh(\mu_{m'}d_1) - g\mu_{m'}}{g\mu_{m'}\tanh(\mu_{m'}d_1) - \omega^2},$$

and a_m, $\bar{a}_m$, b_m^j, $\bar{b}_m^j$, and $c_{m'}^j$, $\bar{c}_{m'}^j$ are the undetermined complex expansion coefficients. Here, the superscript j in b_m^j, $\bar{b}_m^j$, $c_{m'}^j$, $\bar{c}_{m'}^j$, and κ_m^j denotes the j-th subregion, instead of the exponent. The eigenfunctions $Z_m(z)$, $f_{j,m}(z)$, $g_{m'}(x)$ and $\bar{g}_{m'}(x)$ are given by:

$$Z_m(z) = \frac{\cos k_m(z+H)}{\cos(k_m H)}, \quad m = 0, 1, \ldots, \tag{37}$$

$$f_{j,m}(z) = \begin{cases} \dfrac{\cos \lambda_m(z+d_1)}{\cos(\lambda_m d_1)}, & j = 1,\ m = 0, 1, \ldots, \\ \cos \kappa_m^j(z+d_j), & j = 2, 3, \ldots, N+1, \quad m = 0, 1, \ldots, \end{cases} \tag{38}$$

$$g_{m'}(x) = \cos(\mu_{m'} x), \quad m' = 0, 1, \ldots, \tag{39}$$

$$\bar{g}_{m'}(x) = \sin(\mu_{m'} x), \quad m' = 0, 1, \ldots, \tag{40}$$

in which the eigenvalues κ_m^j and $\mu_{m'}$ are written as:

$$\kappa_m^j = \frac{m\pi}{d_j - d_{j-1}} = \frac{m\pi}{h_j}, \quad j = 2, 3, \ldots, N+1,\ m = 0, 1, \ldots, \tag{41}$$

$$\mu_{m'} = \frac{m'\pi}{L} + \frac{\pi}{2L}, \quad m' = 0, 1, \ldots, \tag{42}$$

and the eigenvalues k_m and λ_m are the roots of the following characteristic equations:

$$\omega^2 = -g k_m \tan(k_m H), \quad m = 0, 1, \ldots, \tag{43}$$

$$\omega^2 = -g \lambda_m \tan(\lambda_m d_1), \quad m = 0, 1, \ldots, \tag{44}$$

where $k_0 = \mathrm{i}k$, $\lambda_0 = \mathrm{i}\lambda$. Here, k_0 and λ_0 represent the propagating modes of the corresponding potentials.

It is to be noted that the eigenfunctions have the following orthogonality:

$$\int_{-H}^{0} Z_m(z) Z_n(z)\,\mathrm{d}z = \frac{k_m H \sec^2(k_m H) + \tan(k_m H)}{2k_m}\delta_{mn}, \tag{45}$$

$$\int_{-d_1}^{0} f_{1,m}(z) f_{1,n}(z)\,\mathrm{d}z = \frac{\lambda_m d_1 \sec^2(\lambda_m d_1) + \tan(\lambda_m d_1)}{2\lambda_m}\delta_{mn}, \tag{46}$$

$$\int_{-d_j}^{-d_{j-1}} f_{j,m}(z) f_{j,n}(z)\,\mathrm{d}z = \begin{cases} h_j \delta_{0n}, & m = 0, \\ \dfrac{1}{2} h_j \delta_{mn}, & m = 1, 2, \ldots \end{cases} \quad j = 2, 3, \ldots, N+1, \tag{47}$$

$$\int_{-L}^{0} g_{m'}(x) g_{n'}(x)\,\mathrm{d}x = \int_{-L}^{0} \bar{g}_{m'}(x) \bar{g}_{n'}(x)\,\mathrm{d}x = \frac{1}{2} L \delta_{m'n'}, \tag{48}$$

where δ_{mn} is the Kronecker delta defined as $\delta_{mn} = \begin{cases} 1, & \text{if } m = n, \\ 0, & \text{if } m \neq n. \end{cases}$

Substituting Eqs. (29)–(31) and (33)–(35) into the matching conditions (26)–(28), applying the above orthogonality of the eigenfunctions, and truncating m (m') at M (M'), the algebraic equation sets for symmetrical and anti-symmetrical potentials can be derived, as listed in Appendix 1 and 2, respectively. The $(N+2)(M+1)+N(M'+1)$ unknowns in each algebraic equation set can be obtained thereafter.

The convergence of the systems (57)–(61) and (75)–(79) is slightly slow as M increases because of the singularity at the plate tips revealed by (6). Although the residue calculus technique, which was applied by [35] can obtain a better convergence in solving wave reflection by a finite submerged porous plate, the complex dispersion relation is required. In the present solution, as will be mentioned in Sect. 4.1, the convergence is still reasonably good and could be qualified in engineering practice.

Consequently, the wave reflection coefficient C_R, the transmission coefficient C_T and the energy dissipation coefficient C_D are given as follows:

$$C_\mathrm{R} = \frac{|a_0 + \bar{a}_0|}{2}, \tag{49}$$

$$C_\mathrm{T} = \frac{|a_0 - \bar{a}_0|}{2}, \tag{50}$$

$$C_\mathrm{D} = 1 - C_\mathrm{R}^2 - C_\mathrm{T}^2. \tag{51}$$

In addition, the vertical hydrodynamic force acting on each plate F_j and the corresponding non-dimensional total vertical force coefficient C_{F} are given by the following equations:

$$F_j = \mathrm{i}\rho\omega \int_{-L}^{L} (\phi_{j+1} - \phi_j)\Big|_{z=-d_j} \mathrm{d}x = \mathrm{i}\rho\omega \int_{-L}^{0} \left(\phi^{\mathrm{S}}_{j+1} - \phi^{\mathrm{S}}_{j}\right)\Big|_{z=-d_j} \mathrm{d}x$$

$$= -\frac{\mathrm{i}\rho g\zeta_0}{2kG_j} \sum_{m'=0}^{M'} c^j_{m'} \frac{\sin(\mu_{m'}L)}{\mu_{m'}}, \quad j = 1, 2, \ldots, N, \tag{52}$$

$$C_{\mathrm{F}} = \frac{|\sum_{j=1}^{N} F_j|}{2\rho g\zeta_0 L} = \frac{1}{4kL} \left| \sum_{j=1}^{N} \sum_{m'=0}^{M'} \frac{c^j_{m'}}{G_j} \frac{\sin(\mu_{m'}L)}{\mu_{m'}} \right|, \tag{53}$$

where ρ is the density of water.

3 Experiments

To validate the analytical solutions derived above, a series of experiments were conducted in a two-dimensional wave flume located at State Key Laboratory of Ocean Engineering, Shanghai Jiao Tong University, China. The wave flume is 14 m long, 1 m wide, and 1.2 m deep, with a flap-type wave maker equipped at the one end and a slope wave absorber installed at the other end (as shown in Fig. 2). The horizontal porous plates were mounted on an aluminium frame, which was then fixed to a support beam on the top of the flume through four three-component force transducers. These horizontal plates were 2.0 mm thick, and their stiffness was reinforced by four slender columns in the middle. Applying the three-point method developed by Mansard and Funke [36] to discriminate the incident, reflected and transmitted components, six wave probes were used in the test, with three in front of the model and the others downstream. The spacing between adjacent wave probes was set at 0.15 and 0.22 m, respectively, to eliminate singularities.

In the tests, the water depth H was 0.8 m, and the wave periods T ranged from 0.6 to 1.5 s (the corresponding dimensionless wave numbers kH ranged between 8.95 and 1.56). An incident wave height of 2 cm was applied in the tests. The full width of the breakwater $2L$ was 0.45 m. Models with four and eight layers were tested. The plate porosity P was 0.125, of which the corresponding porosity parameter G was approximately 0.992 according to the empirical formula $G = (57.63P - 0.9717)/(2\pi)$ (see [10]). The submerged depth of each horizontal plate is listed in Table 1.

The frequency of each regular wave and the relative phase differences at wave probes were estimated by the FFT (Fast Fourier Transform) technique with Hann window and an interpolation algorithm by Andria et al. [37]. Higher harmonics induced by the submerged horizontal plates were not considered in the data analysis and were filtered out. Then the least squares method by Mansard and Funke [36] was applied to evaluate the incident wave height ζ_{I}, reflected wave height ζ_{R}, and transmitted wave height ζ_{T}. The amplitude of total vertical wave force F_{Z} can be

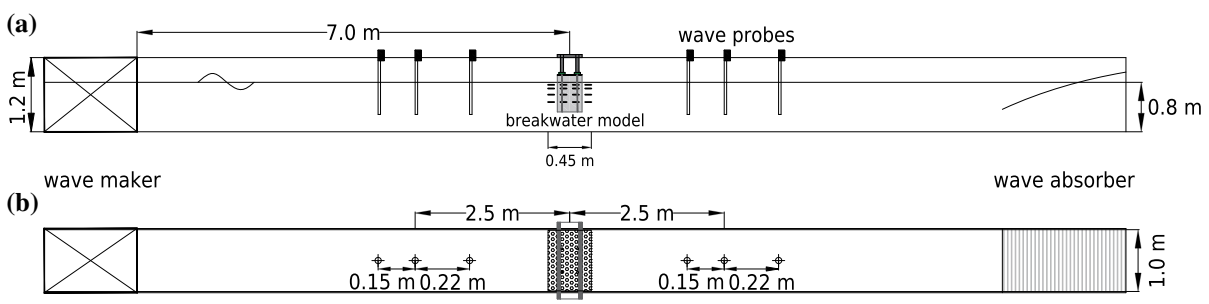

Fig. 2 Sketch of the experimental setup: **a** side view and **b** top view

Table 1 Submerged depths of the horizontal plates

Model no.	N	d_i (cm)
1	4	4, 10, 20, 32
2	8	4, 8, 12, 16, 20, 24, 28, 32

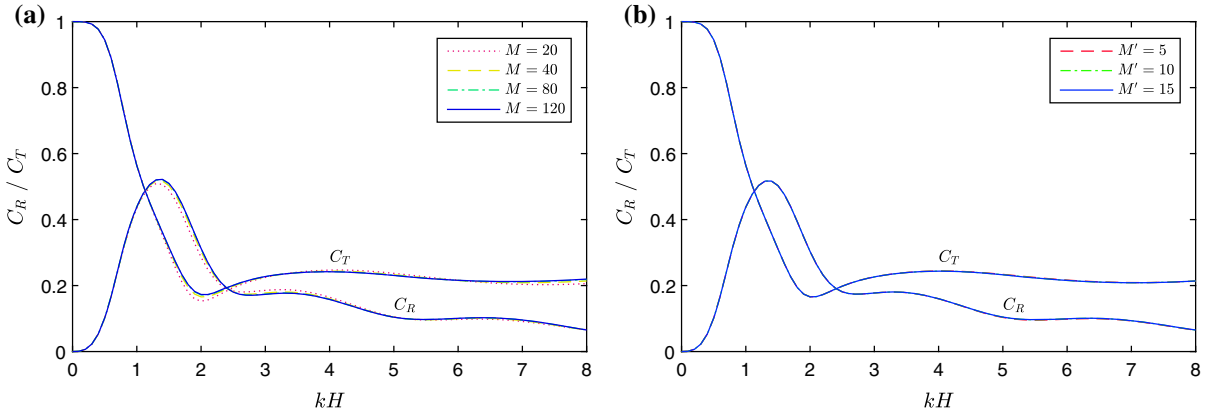

Fig. 3 Convergence of C_{R} and C_{T} with increasing values of truncated numbers M and M', respectively, as the function of non-dimensional wave number kH (at $2L/H = 1$, $d_j/H = 0.08, 0.16, 0.24, 0.32$, $G_j = 1.0, 0.8, 0.6, 0.4$). **a** Increasing M (given $M' = 10$). **b** Increasing M' (given $M = 40$)

obtained using the four three-component force transducers and the FFT technique. Thereafter, the hydrodynamic coefficients of the breakwater (i.e., C_{R}, C_{T}, and C_{F}) can be given as follows:

$$C_{\mathrm{R}} = \frac{\zeta_{\mathrm{R}}}{\zeta_{\mathrm{I}}}, \tag{54}$$

$$C_{\mathrm{T}} = \frac{\zeta_{\mathrm{T}}}{\zeta_{\mathrm{I}}}, \tag{55}$$

$$C_{\mathrm{F}} = \frac{F_{\mathrm{Z}}}{2\rho g \zeta_I L W}, \tag{56}$$

in which W is the flume width.

4 Results and discussions

4.1 Validation of present solution

The convergence of the solutions with different truncated numbers M and M' was examined first, and the results of the reflection and transmission coefficients are shown in Fig. 3. It can be seen that the convergence is acceptable and that values of $M = 40$ and $M' = 10$ should be sufficient for engineering purposes. Therefore, the values of $M = 40$ and $M' = 10$ were adopted in the present study.

The generalized analytical solution to multi-layer horizontal porous plates was consistent with the results of special cases such as the single layer case [23] and the double layer case [24] because of the similar solution technique. In addition, the present solution was validated by comparing the calculation results of cases corresponding with the measured values of the physical model tests described in Sect. 3. The transmission coefficient C_{T}, the reflection coefficient C_{R} and the total vertical force coefficient C_{F} of the four-layer breakwater are shown in Fig. 4a–c, respectively. Furthermore, Fig. 4d–f show those of the eight-layer case. The predicted hydrodynamic performance of the breakwater is in reasonable concordance with that obtained from the experiment, though there exist slight

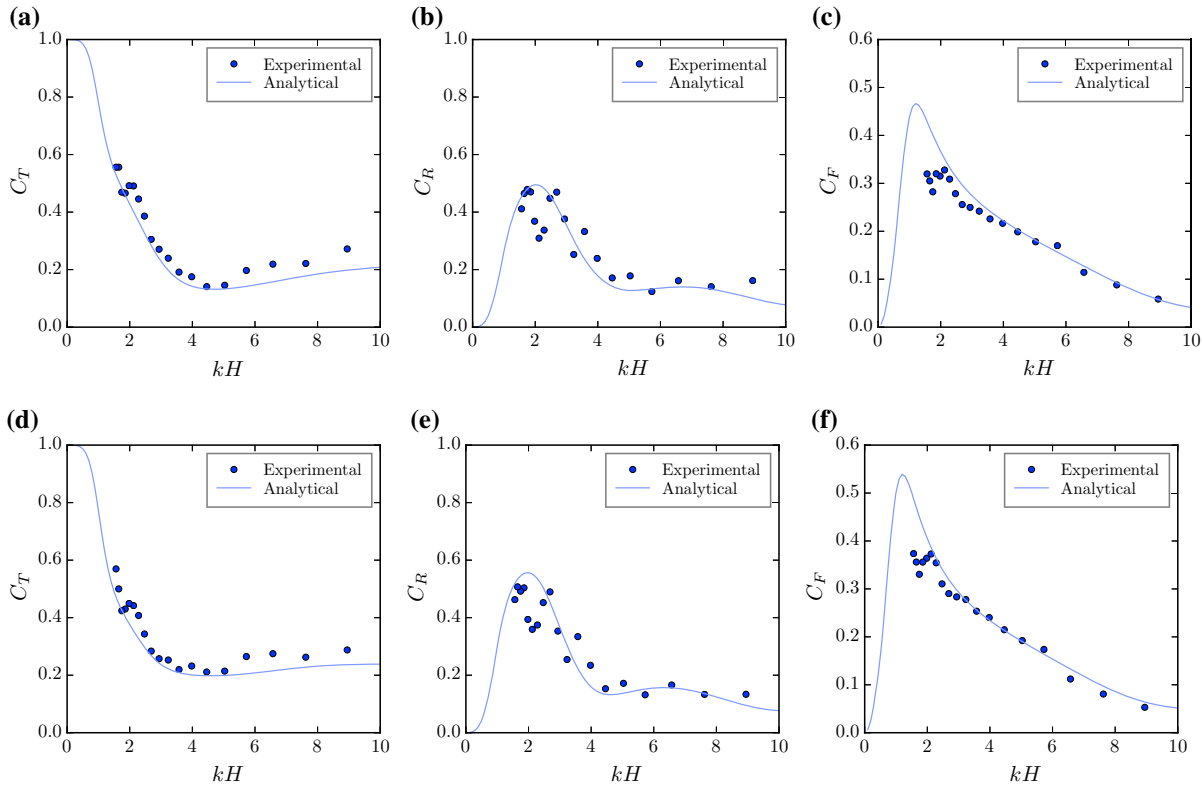

Fig. 4 Comparison between the analytical results and experimental values: **a–c** C_T, C_R and C_F of the four-layer case (Model No. 1); **d–f** C_T, C_R and C_F of the eight-layer case (Model No. 2)

discrepancies between the results. The discrepancies are mainly resulted by the nonlinear effects of free surface and porous plates, which were not taken into consideration in the analytical solution based on the linear potential theory. The small fluctuation of measured values of C_R and C_T around the predicted curve can be attributed to the nonlinearity of the free surface and the shoaling effect of the upper plate. In addition, the slight discrepancy of C_R and C_F under long incident wave periods (i.e., kH around 2) is probably brought on by the turbulence issued from the porous plates.

4.2 Computed velocity fields

Based on the generalized analytical solution, the velocity fields were computed. The potential theory can provide reasonable description of the velocity fields away from the plate tips where the flow separation and vortex shedding might have notable influences. Figure 5 shows an example of the velocity fields of the three-layer horizontal porous plate breakwater for $d_j/H = 0.05,\ 0.15,\ 0.3$, $G_j = 1.2,\ 0.8,\ 0.5$, $2L/H = 1$, and $kH = 2$. The time t_0 is chosen at the beginning of a wave cycle, and T denotes the incident wave period. The velocities are nondimensionalized by $gk\zeta_0/(2\omega)$. As comparison, Fig. 6 shows the cases of breakwaters with only one or two layer(s) at $t = t_0 + T/4$.

It is observed in Fig. 5 that the horizontal porous plates change the original velocity fields significantly and the vertical motion of fluid particles is obstructed. Large amplitudes of fluid motion near the free surface are attenuated. The flow beneath the lower plate is almost horizontal. The downstream flow is weak except in the vicinity of the breakwater where the influence of the evanescent waves is significant. Since the amplitude of fluid velocity in the region above the upper plate is notably larger than that in the regions below it, a substantial proportion of wave energy propagates through the region above the upper plate. Therefore, the upper plate is expected to

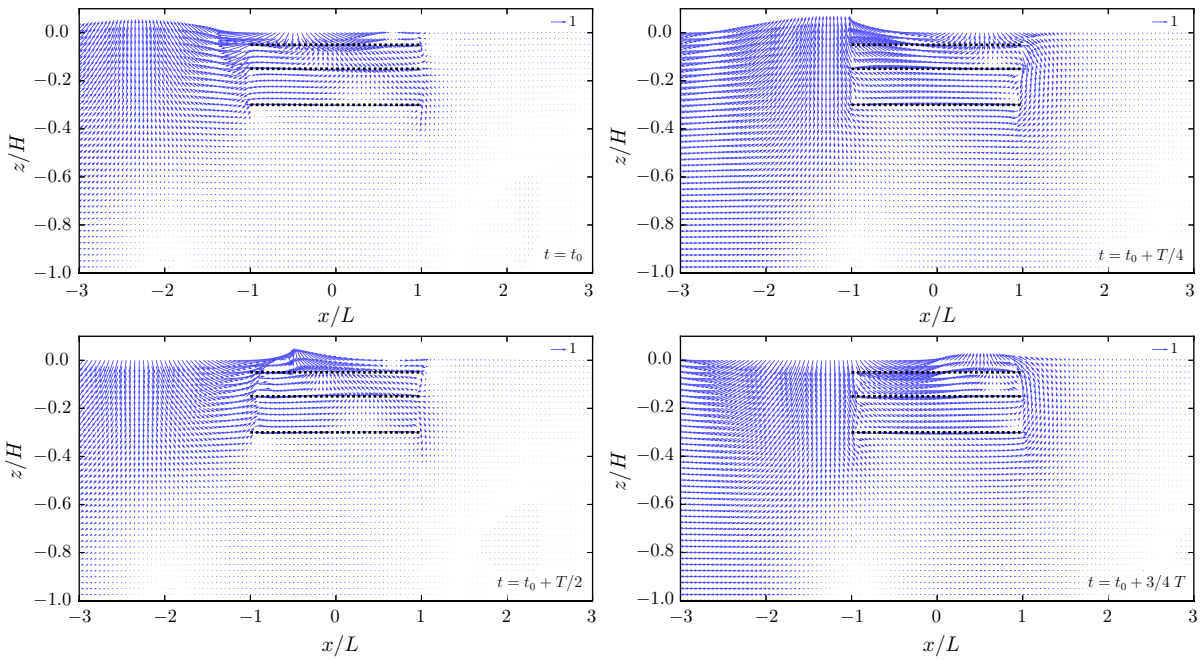

Fig. 5 Velocity fields of the three-layer submerged horizontal porous plate breakwater, for $d_j/H = 0.05,\ 0.15,\ 0.3, G_j = 1.2,\ 0.8,\ 0.5,$ $2L/H = 1$, and $kH = 2$

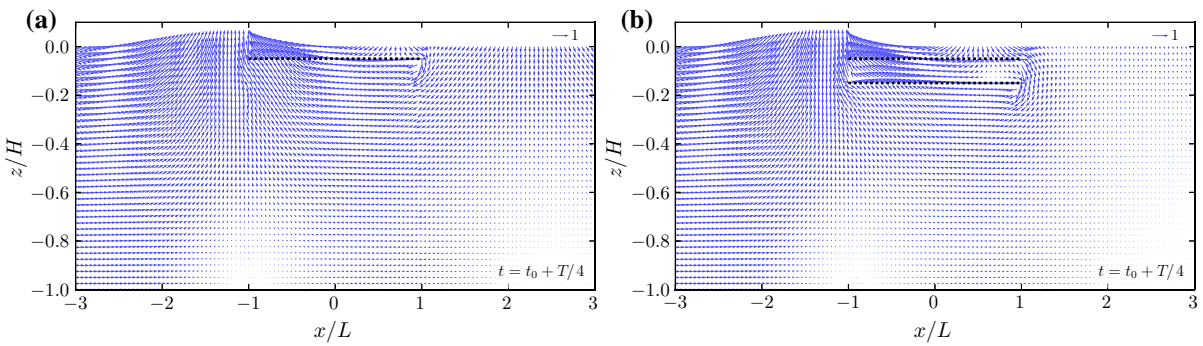

Fig. 6 Velocity fields of the **a** one- and **b** two-layer submerged horizontal porous plate breakwater at $kH = 2$ and $t = t_0 + T/4$, for **a** $d/H = 0.05, G = 1.2, 2L/H = 1$, and **b** $d_j/H = 0.05,\ 0.15, G_j = 1.2,\ 0.8, 2L/H = 1$

play a more important role in wave dissipation than any other plates, and changes in its submergence or porosity might significantly affect the breakwater's performance. In the region between the upper and the second plates, the direction of the flow is changed and becomes more horizontal, in comparison with that in the case of only one layer (shown in Fig. 6a). Comparing to the two-layer case shown in Fig. 6b, the lower plate in the three-layer case can reinforce the obstruction of the vertical fluid motion, but its porosity might have minimal effect on the performance because the seepage flow is relatively small.

4.3 Effects of submerged depth and porous parameter

To illustrate the effect of different submerged depths and porous parameters on the wave-blocking performance of the horizontal plates, a three-layer breakwater was taken as an example.

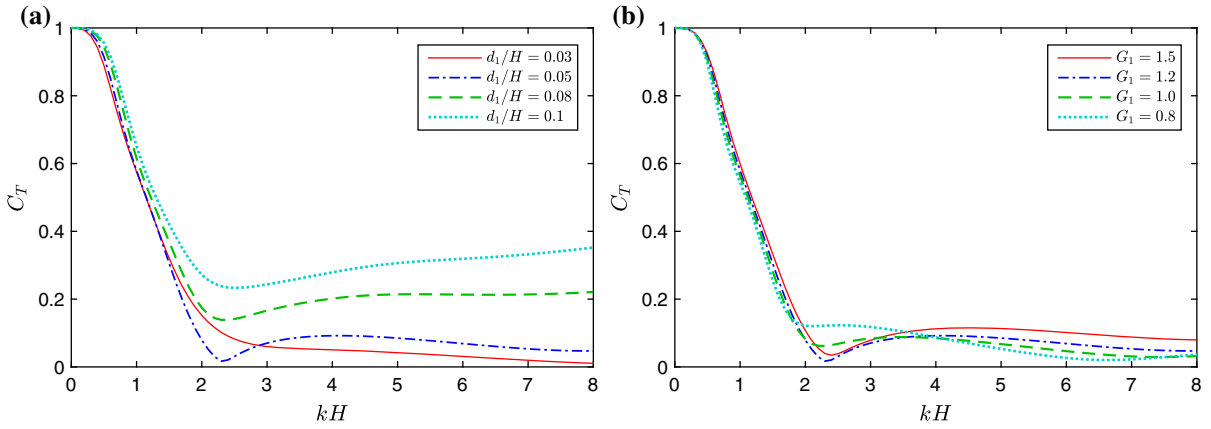

Fig. 7 C_T of three-layer submerged horizontal porous-plate breakwaters, as a function of the non-dimensional wave number kH, for $2L/H = 1$, $G_2 = 0.8$, $G_3 = 0.5$, $(d_2 - d_1)/H = 0.1$, $(d_3 - d_2)/H = 0.15$ with **a** varying values of d_1 and with fixed $G_1 = 1.2$ and **b** varying values of G_1 and with fixed $d_1/H = 0.05$

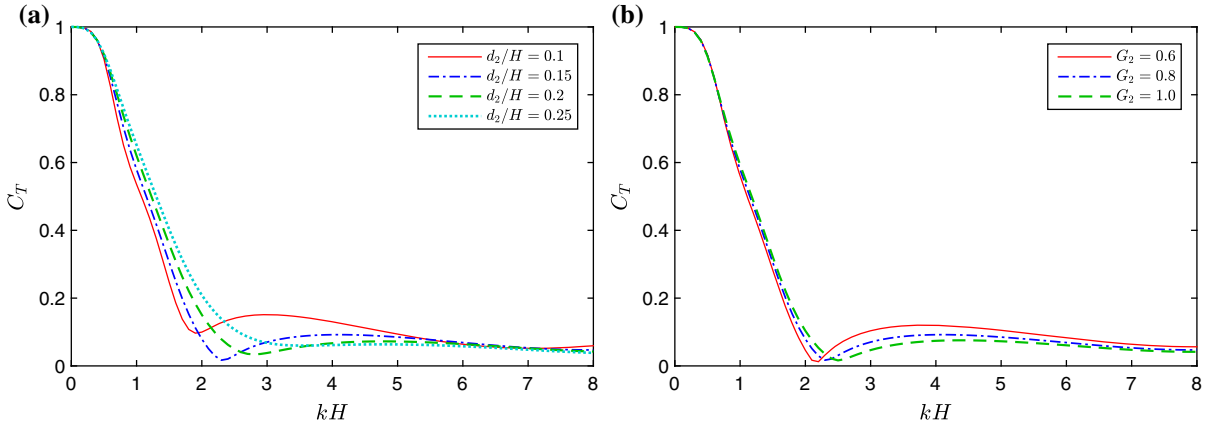

Fig. 8 C_T of three-layer submerged horizontal porous-plate breakwaters, as a function of the non-dimensional wave number kH, for $2L/H = 1$, $G_1 = 1.2$, $G_3 = 0.5$, $d_1/H = 0.05$, $(d_3 - d_2)/H = 0.15$ with **a** varying values of d_2 and with fixed $G_2 = 0.8$ and **b** varying values of G_2 and with fixed $d_2/H = 0.15$

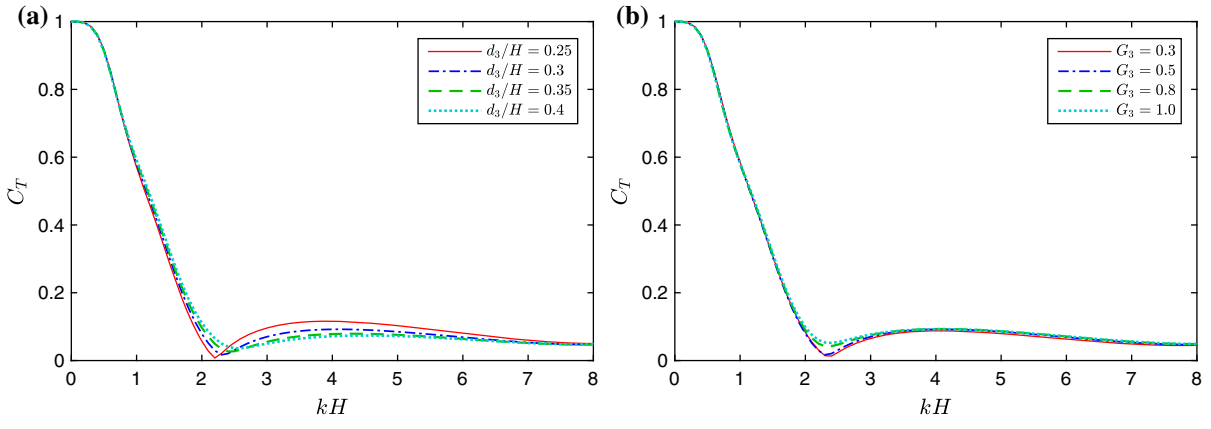

Fig. 9 C_T of three-layer submerged horizontal porous plates breakwaters, as a function of the non-dimensional wave number kH for $2L/H = 1$, $G_1 = 1.2$, $G_2 = 0.8$, $d_1/H = 0.05$, $d_2/H = 0.15$ with **a** varying values of d_3 and with fixed $G_3 = 0.5$ and **b** varying values G_3 and with fixed $d_3/H = 0.3$

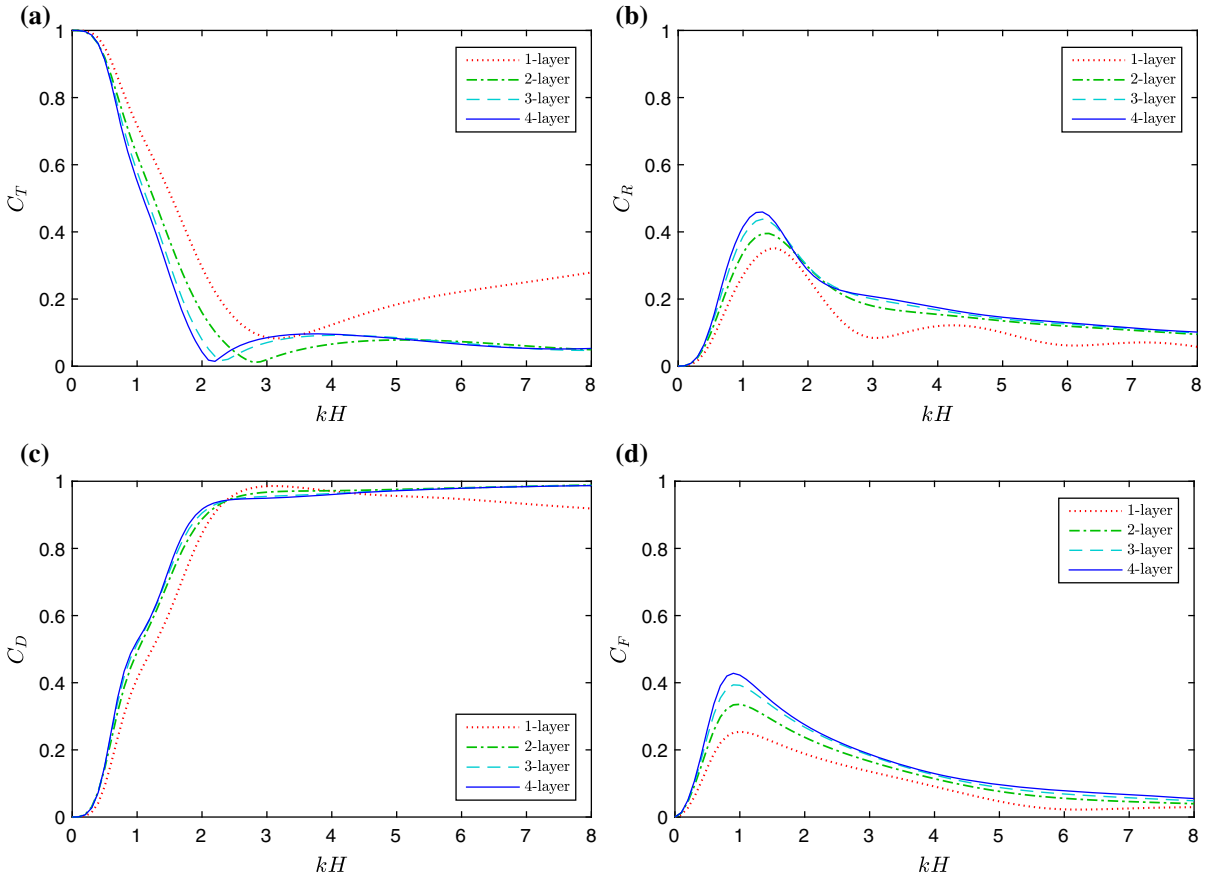

Fig. 10 C_{T}, C_{R}, C_{D}, and C_{F} of breakwaters with one to four layers of horizontal porous plates, as a function of non-dimensional wave number kH at $2L/H = 1$. For the single layer case, $d/H = 0.1$ and $G = 0.8$; for the double layer case, $d_j/H = 0.05, 0.2, G_j = 1.2, 0.6$; for the three-layer case, $d_j/H = 0.05, 0.15, 0.3, G_j = 1.2, 0.8, 0.5$; for the four-layer case, $d_j/H = 0.05, 0.13, 0.25, 0.40, G_j = 1.2, 0.8, 0.6, 0.3$. **a** wave transmission coefficient C_{T}. **b** wave reflection coefficient C_{R}. **c** wave energy dissipation coefficient C_{D}. **d** total wave force coefficient C_F

Figure 7 individually compares the effect on the wave-blocking efficiency of different submerged depths and porous parameters of the upper plate, for $2L/H = 1, G_2 = 0.8, G_3 = 0.5, (d_2-d_1)/H = 0.1, (d_3-d_2)/H = 0.15$. In Fig. 7a, G_1 is provisionally set at 1.2, and in Fig. 7b d_1/H is set at 0.05. The significant effect of the upper plate submergence on the overall wave-blocking efficiency of the breakwater is observed as expected. A relatively large d_1 may weaken the wave-blocking effect, especially for moderate and short incident wave lengths ($kH > 3$), because this allows more wave energy to propagate above the upper plate. For the porous parameter of the upper plate, a large value may worsen the performance under $kH > 4$, which might relate to the energy-attenuating effect of porosity on the seepage flow through the plate. Generally, values of $d_1/H = 0.05$ and $G_1 = 1.2$ provide optimal performance.

The individual effects of the varying submerged depth and porous parameter of the middle plate, are shown in Fig. 8, for $2L/H = 1, d_1/H = 0.05, (d_3 - d_2)/H = 0.15, G_1 = 1.2, G_3 = 0.5$. In Fig. 8a, G_2 is set at 0.8 while d_2/H varies from 0.1 to 0.25. In Fig. 8b, d_2/H is set at 0.1 while G_2 varies from 0.6 to 1.0. A smaller spacing between the upper and middle plates reduces the wave transmission under $kH \leq 2$, but worsens the wave-blocking efficiency under moderate incident wave lengths ($2 \leq kH \leq 4$). For the middle plate, the effect of its porous parameter is less significant than that of the submerged depth. A smaller G_2 helps reduce the wave transmission under $kH \leq 2$, but it has an opposite effect under $kH \geq 2.5$. It can be seen in Fig. 8 that values of $d_2 = 0.15$ and $G_2 = 0.8$ should produce generally good wave-blocking performance.

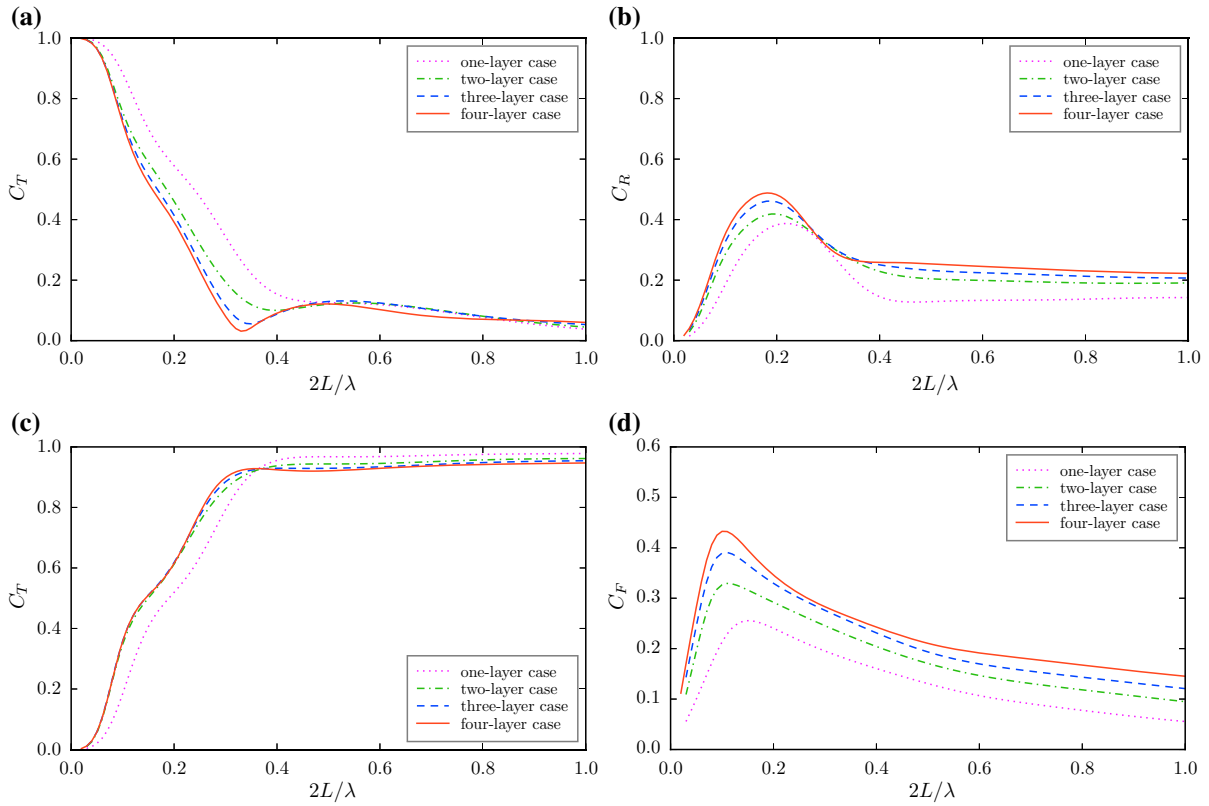

Fig. 11 C_T, C_R, C_D, and C_F of breakwaters with different plate widths at $kH = 2.0$, as a function of the non-dimensional plate width $2L/\lambda$, for cases of one to four layers. For the single-layer breakwater, $d/H = 0.1$, $G = 0.8$. For the double-layer breakwater, $d_j/H = 0.05,\ 0.2$, $G_j = 1.2,\ 0.6$. For the three-layer breakwater, $d_j/H = 0.05,\ 0.15,\ 0.3$, $G_j = 1.2,\ 0.8,\ 0.5$. For the four-layer breakwater, $d_j/H = 0.05,\ 0.13,\ 0.25,\ 0.4$, $G_j = 1.2,\ 0.8,\ 0.6,\ 0.3$. **a** wave transmission coefficient C_T. **b** wave reflection coefficient C_R. **c** wave energy dissipation coefficient C_D. **d** total wave force coefficient C_F

In accordance with the discussion in Sect. 4.2, varying the submerged depth or the porous parameter of the lower plate only has a mild effect on the wave-blocking efficiency, as shown in Fig. 9, for $2L/H = 1$, $G_1 = 1.2$, $G_2 = 0.8$, $d_1/H = 0.05$, $d_2/H = 0.15$. In Fig. 9a, d_3/H varies from 0.25 to 0.4 with $G_3 = 0.5$, and in Fig. 9b, $d_3/H = 0.3$ while G_3 varies from 0.3 to 1.0. As shown in the results, it is reasonable to take $d_3/H = 0.3$ and $G_3 = 0.5$ for optimal performance.

4.4 Effects of numbers of layers

A comparison between the performances of breakwaters with one to four layers of horizontal porous plates is shown in Fig. 10. The submerged depth and porosity parameters for the different cases are determined by a simple optimization design process that is described below. For the single layer case, $d_1/H = 0.1$ and $G_1 = 0.8$; for the double layer case, $d_1/H = 0.05$, $d_2/H = 0.2$, $G_1 = 1.2$ and $G_2 = 0.6$; for the three-layer case, $d_1/H = 0.05$, $d_2/H = 0.15$, $d_3/H = 0.3$, $G_1 = 1.2$, $G_2 = 0.8$ and $G_3 = 0.5$; and for the four-layer case, $d_1/H = 0.05$, $d_2/H = 0.13$, $d_3/H = 0.25$, $d_4/H = 0.4$, $G_1 = 1.2$, $G_2 = 0.8$, $G_3 = 0.6$ and $G_4 = 0.3$. As can be seen in the figure, breakwaters with three or four horizontal porous plates have better wave-dissipating efficiency, especially under longer incident waves. This indicates that the lower plates indeed help obstruct the vertical fluid motion. However, increasing the layer number also results in a larger total wave force and reflection wave amplitude, and a more sophisticated optimization design is required.

In this paper, the optimization design process simply lowers the transmission coefficient, especially under $1.5 \leq kH \leq 4$. As expounded in Sect. 4.3, each parameter is determined accordingly from a specified range, while other parameters are fixed, and the crucial parameter, such as the submerged depth of the upper plate, is determined first. Additionally, a future study is expected to include the application of some advanced optimization algorithms, such as genetic algorithm, to design the multi-layer horizontal porous plate breakwater while accounting for comprehensive performance including wave reflection and loads on the plates.

4.5 Effects of plate width

Finally, the effects of different plate widths on the hydrodynamic performance of breakwaters with one to four layers of horizontal porous plate(s) were examined at a fixed non-dimensional incident wave number $kH = 2$, as shown in Fig. 11. For the single-layer breakwater, $d_1/H = 0.1$, $G_1 = 0.8$. For the double-layer breakwater, $d_1/H = 0.05$, $d_2/H = 0.2$, $G_1 = 1.2$, $G_2 = 0.6$. For the three-layer breakwater, $d_1/H = 0.05$, $d_2/H = 0.15$, $d_3/H = 0.3$, $G_1 = 1.2$, $G_2 = 0.8$, $G_3 = 0.5$. For the four-layer breakwater, $d_1/H = 0.05$, $d_2/H = 0.13$, $d_3/H = 0.25$, $d_4/H = 0.4$, $G_1 = 1.2$, $G_2 = 0.8$, $G_3 = 0.6$, $G_4 = 0.3$. It is clear that the breakwater can maintain its efficiency quite well until the width is smaller than 0.2λ, where λ denotes the incident wave length. This implied that the breakwater with too large width might be unnecessary under certain prevailing wave climates. For breakwaters with small width, increasing the layer number and extending the covered water depth help to reflect more incident waves and reduce the transmission coefficient. However, an unavoidable fact is that the breakwater tends to become inefficient when its width is smaller than 0.2λ because of the diffraction effect of waves, which may be one of the main limitations of horizontal porous-plate breakwaters.

5 Conclusions

A generalized analytical solution for wave interaction with multi-layer submerged horizontal porous-plate breakwaters has been derived in the context of linear potential theory with the viscous effect based on Darcy's law. A representative two-dimensional model with N layers of horizontal porous plates was considered. The spatial velocity potentials were solved by means of the matched eigenfunction expansion method, and the parameters of the performance that are of concern to engineering practice were subsequently obtained. Techniques based on the geometrical symmetry and on the use of artificial potential splitting were employed to simplify the solution process, as well as to avoid complex dispersion relations. The analytical solution was validated with reasonable agreement compared to the measured values of the corresponding physical model tests.

Thereafter, based on the analytical solution, the velocity fields were computed, and effects of the various parameters (i.e., plate submergence, width, porosity, layer number, and wave parameter) on the breakwater's performance were examined, taking a three-layer horizontal porous plate breakwater for example. The vertical motion of fluid particles is significantly obstructed by the horizontal plates. Large amplitudes of fluid motion near the free surface are attenuated. The flow beneath the lower plate is almost horizontal. The submerged depth of the upper plate has the most significant influence on the overall performance. The lower plate can reinforce the obstruction of the vertical fluid motion. Breakwaters with three or more layers of horizontal plates have better wave-blocking performance, especially under long incident waves. Nevertheless, horizontal porous plate breakwaters may become inefficient if the plate width is less than 0.2λ.

The generalized analytical solution provides an effective tool for predicting and optimizing the performance of the multi-layer horizontal porous plate breakwater. A simple procedure for the optimization design aiming at reducing the wave transmission was discussed. Based on the generalized solution, further optimization of its comprehensive performance using some advanced algorithms, e.g., genetic algorithm, is expected. Methods for improving the performance under relatively small plate widths warrant further study.

Acknowledgements The authors would like to acknowledge the support of the National Natural Science Foundation of China (Grant No. 51239007). The authors are also grateful to the anonymous reviewers whose valuable comments and suggestions have contributed to improving the manuscript.

Appendix 1: Elements in coefficient matrices for symmetrical potentials

The algebraic equation set for the symmetrical potentials is given by:

$$\left[A_{nm}^{j}\right]\{a_m\}+\left\{b_n^{j}\right\}=\left\{R_n^{j}\right\},\quad j=1,2,\ldots,N+1, \tag{57}$$

$$\{a_n\}+\sum_{j=1}^{N+1}\left[B_{nm}^{j}\right]\left\{b_m^{j}\right\}+\sum_{j=1}^{N}\left[C_{nm'}^{j}\right]\left\{c_{m'}^{j}\right\}=\left\{R_n^{N+2}\right\}. \tag{58}$$

$$\left[D_{n'm}^{1,1}\right]\left\{b_m^{1}\right\}+\left[D_{n'm}^{1,2}\right]\left\{b_m^{2}\right\}+\left[E_{n'm'}^{1,1}\right]\left\{c_{m'}^{1}\right\}+\left[E_{n'm'}^{1,2}\right]\left\{c_{m'}^{2}\right\}=0, \tag{59}$$

$$\left[D_{n'm}^{j,j}\right]\left\{b_m^{j}\right\}+\left[D_{n'm}^{j,j+1}\right]\left\{b_m^{j+1}\right\}+\left[E_{n'm'}^{j,j-1}\right]\left\{c_{m'}^{j-1}\right\}+\left[E_{n'm'}^{j,j}\right]\left\{c_{m'}^{j}\right\}+\left[E_{n'm'}^{j,j+1}\right]\left\{c_{m'}^{j+1}\right\}=0,\quad j=2,3,\ldots,N-1, \tag{60}$$

$$\left[D_{n'm}^{N,N}\right]\left\{b_m^{N}\right\}+\left[D_{n'm}^{N,N+1}\right]\left\{b_m^{N+1}\right\}+\left[E_{n'm'}^{N,N-1}\right]\left\{c_{m'}^{N-1}\right\}+\left[E_{n'm'}^{N,N}\right]\left\{c_{m'}^{N}\right\}=0, \tag{61}$$

where $[\cdot]$ denotes a matrix and $\{\cdot\}$ denotes a column vector. The matrix elements are given by

$$A_{nm}^{j}=\frac{\int_{-d_j}^{-d_{j-1}}Z_m(z)f_{j,n}(z)\,\mathrm{d}z}{-\int_{-d_j}^{-d_{j-1}}\left(f_{j,n}(z)\right)^2\,\mathrm{d}z},\quad j=1,2,\ldots,N+1, \tag{62}$$

$$B_{nm}^{j}=\begin{cases}\lambda_m\tanh\lambda_m L\dfrac{\int_{-d_1}^{0}Z_n(z)f_{1,m}(z)\,\mathrm{d}z}{\tilde{k}_n\int_{-H}^{0}(Z_n(z))^2\,\mathrm{d}z}, & j=1,\\ \kappa_m^{j}\tanh\kappa_m^{j}L\dfrac{\int_{-d_j}^{-d_{j-1}}Z_n(z)f_{j,m}(z)\,\mathrm{d}z}{\tilde{k}_n\int_{-H}^{0}(Z_n(z))^2\,\mathrm{d}z}, & j=2,3,\ldots,N+1,\end{cases} \tag{63}$$

$$C_{nm}^{j}=\begin{cases}-\dfrac{\sin\mu_{m'}L\left\{\begin{array}{l}\int_{-d_1}^{0}Z_n(z)\left(\eta_{m'}\cosh\mu_{m'}(z+d_1)+\sinh\mu_{m'}(z+d_1)\right)\,\mathrm{d}z\\ \quad+\int_{-d_2}^{-d_1}Z_n(z)\frac{\cosh\mu_{m'}(z+d_2)}{\sinh(\mu_{m'}h_2)}\,\mathrm{d}z\end{array}\right\}}{\tilde{k}_n\int_{-H}^{0}(Z_n(z))^2\,\mathrm{d}z}, & j=1,\\ \dfrac{\sin\mu_{m'}L\left[\int_{-d_j}^{-d_{j-1}}Z_n(z)\frac{\cosh\mu_{m'}(z+d_{j-1})}{\sinh(\mu_{m'}h_j)}\,\mathrm{d}z-\int_{-d_{j+1}}^{-d_j}Z_n(z)\frac{\cosh\mu_{m'}(z+d_{j+1})}{\sinh(\mu_{m'}h_{j+1})}\,\mathrm{d}z\right]}{\tilde{k}_n\int_{-H}^{0}(Z_n(z))^2\,\mathrm{d}z}, & j=2,3,\ldots,N,\end{cases} \tag{64}$$

$$D_{n'm}^{j,j}=\begin{cases}\dfrac{k_0G_1}{\cos(\lambda_m d_1)}\displaystyle\int_{-L}^{0}\frac{\cosh(\lambda_m x)}{\cosh(\lambda_m L)}\cos(\mu_{n'}x)\,\mathrm{d}x, & j=1,\\ k_0G_j\displaystyle\int_{-L}^{0}\frac{\cosh(\kappa_m^{j}x)}{\cosh(\kappa_m^{j}L)}\cos(\mu_{n'}x)\,\mathrm{d}x, & j=2,3,\ldots,N,\end{cases} \tag{65}$$

$$D_{n'm}^{j,j+1}=-k_0G_j\cos\left(\kappa_m^{j+1}h_{j+1}\right)\int_{-L}^{0}\frac{\cosh(\kappa_m^{j+1}x)}{\cosh(\kappa_m^{j+1}L)}\cos(\mu_{n'}x)\,\mathrm{d}x,\quad j=1,2,\ldots,N, \tag{66}$$

$$E_{n'm'}^{j,j-1}=\frac{L}{2}G_j\beta_{n'}^{j}\delta_{n'm'},\quad j=2,3,\ldots,N, \tag{67}$$

$$E_{n'm'}^{j,j}=\begin{cases}\dfrac{L}{2}\alpha_{n'}\delta_{n'm'}, & j=1,\\ \dfrac{L}{2}\gamma_{n'}^{j}\delta_{n'm'}, & j=2,3,\ldots,N,\end{cases} \tag{68}$$

$$E^{j,j+1}_{n'm'} = \frac{L}{2} G_j \beta^{j+1}_{n'} \delta_{n'm'}, \quad j = 1, 2, \ldots, N-1, \tag{69}$$

$$R^j_n = \frac{\int_{-d_j}^{-d_{j-1}} Z_0(z) f_{j,n}(z)\, \mathrm{d}z}{\int_{-d_j}^{-d_{j-1}} \left(f_{j,n}(z)\right)^2\, \mathrm{d}z}, \quad j = 2, 3, \ldots, N+1, \tag{70}$$

$$R^{N+2}_n = \delta_{n0}. \tag{71}$$

Here, $\alpha_{m'}$, $\beta^j_{m'}$ and $\gamma^j_{m'}$ are given by:

$$\alpha_{m'} = 1 + \mathrm{i}kG_1 \left(\frac{\eta_{m'}}{\mu_{m'}} - \frac{\coth\left(\mu_{m'} h_2\right)}{\mu_{m'}} \right), \tag{72}$$

$$\beta^j_{m'} = \frac{\mathrm{i}k}{\mu_{m'} \sinh\left(\mu_{m'} h_j\right)}, \tag{73}$$

$$\gamma^j_{m'} = 1 - \mathrm{i}kG_j \left(\frac{\coth\left(\mu_{m'} h_j\right)}{\mu_{m'}} + \frac{\coth\left(\mu_{m'} h_{j+1}\right)}{\mu_{m'}} \right), \tag{74}$$

and $\tilde{k}_n$ is defined by $\tilde{k}_n = \begin{cases} -k_0, & n = 0, \\ k_n, & n = 1, 2, \ldots \end{cases}$

Appendix 2: Elements in coefficient matrices for anti-symmetrical potentials

The algebraic equation set for the anti-symmetrical potentials is given by

$$\{\bar{a}_n\} + \sum_{j=1}^{N+1} \left[\overline{B}^j_{nm}\right] \left\{\bar{b}^j_n\right\} + \sum_{j=1}^{N} \left[\overline{C}^j_{nm'}\right] \left\{\bar{c}^j_{m'}\right\} = \left\{\overline{R}^1_n\right\}, \tag{75}$$

$$\left[\overline{A}^j_{nm}\right] \{\bar{a}_m\} + \left\{\bar{b}^j_n\right\} = \left\{\overline{R}^{1+j}_n\right\}, \quad j = 1, 2, \ldots, N+1, \tag{76}$$

$$\left[\overline{D}^{1,1}_{n'm}\right] \left\{\bar{b}^1_m\right\} + \left[\overline{D}^{1,2}_{n'm}\right] \left\{\bar{b}^2_m\right\} + \left[\overline{E}^{1,1}_{n'm'}\right] \left\{\bar{c}^1_{m'}\right\} + \left[\overline{E}^{1,2}_{n'm'}\right] \left\{\bar{c}^2_{m'}\right\} = 0, \tag{77}$$

$$\left[\overline{D}^{j,j}_{n'm}\right] \left\{\bar{b}^j_m\right\} + \left[\overline{D}^{j,j+1}_{n'm}\right] \left\{\bar{b}^{j+1}_m\right\} + \left[\overline{E}^{j,j-1}_{n'm'}\right] \left\{\bar{c}^{j-1}_{m'}\right\} + \left[\overline{E}^{j,j}_{n'm'}\right] \left\{\bar{c}^{j}_{m'}\right\} + \left[\overline{E}^{j,j+1}_{n'm'}\right] \left\{\bar{c}^{j+1}_{m'}\right\} = 0$$
$$j = 2, 3, \ldots, N-1, \tag{78}$$

$$\left[\overline{D}^{N,N}_{n'm}\right] \left\{\bar{b}^N_m\right\} + \left[\overline{D}^{N,N+1}_{n'm}\right] \left\{\bar{b}^{N+1}_m\right\} + \left[\overline{E}^{N,N-1}_{n'm'}\right] \left\{\bar{c}^{N-1}_{m'}\right\} + \left[\overline{E}^{N,N}_{n'm'}\right] \left\{\bar{c}^{N}_{m'}\right\} = 0. \tag{79}$$

The matrix elements in Eqs. (75)–(79) are given by

$$\overline{A}^1_{nm} = \frac{\tilde{k}_m \int_{-d_1}^{0} Z_m(z) f_{1,n}(z)\, \mathrm{d}z}{\lambda_n \coth(\lambda_n L) \int_{-d_1}^{0} \left(f_{1,n}(z)\right)^2\, \mathrm{d}z}, \tag{80}$$

$$\overline{A}^j_{nm} = \begin{cases} \dfrac{\tilde{k}_m L \int_{-d_j}^{-d_{j-1}} Z_m(z)\, \mathrm{d}z}{h_j}, & n = 0, \\ \dfrac{2\tilde{k}_m \int_{-d_j}^{-d_{j-1}} Z_m(z) f_{j,n}(z)\, \mathrm{d}z}{h_j \kappa^j_n \coth(\kappa^j_n L)}, & n = 1, 2, \ldots, M, \end{cases} \quad j = 2, 3, \ldots, N+1, \tag{81}$$

$$\overline{B}^j_{nm} = -\frac{\int_{-d_j}^{-d_{j-1}} Z_n(z) f_{j,m}(z)\, \mathrm{d}z}{\int_{-H}^{0} \left(Z_n(z)\right)^2\, \mathrm{d}z}, \quad j = 1, 2, \ldots, N+1, \tag{82}$$

$$\overline{C}^{j}_{nm'} = \begin{cases} \dfrac{\sin\mu_{m'}L\left\{\begin{array}{l}\int_{-d_1}^{0} Z_n(z)\left(\eta_{m'}\cosh\mu_{m'}(z+d_1)+\sinh\mu_{m'}(z+d_1)\right)\,\mathrm{d}z \\ \quad +\int_{-d_2}^{-d_1} Z_n(z)\frac{\cosh\mu_{m'}(z+d_2)}{\sinh(\mu_{m'}h_2)}\,\mathrm{d}z\end{array}\right\}}{\mu_{m'}\int_{-H}^{0}(Z_n(z))^2\,\mathrm{d}z}, & j=1, \\ \dfrac{\sin\mu_{m'}L\left[\int_{-d_{j+1}}^{-d_j} Z_n(z)\frac{\cosh\mu_{m'}(z+d_{j+1})}{\sinh(\mu_{m'}h_{j+1})}\,\mathrm{d}z-\int_{-d_j}^{-d_{j-1}} Z_n(z)\frac{\cosh\mu_{m'}(z+d_{j-1})}{\sinh(\mu_{m'}h_j)}\,\mathrm{d}z\right]}{\mu_{m'}\int_{-H}^{0}(Z_n(z))^2\,\mathrm{d}z}, & j=2,3,\ldots,N, \end{cases} \tag{83}$$

$$\overline{D}^{1,1}_{n'm} = \frac{-k_0G_1}{\cos(\lambda_m d_1)}\int_{-L}^{0}\frac{\sinh(\lambda_m x)}{\sinh(\lambda_m L)}\sin(\mu_{n'}x)\,\mathrm{d}x, \tag{84}$$

$$\overline{D}^{j,j}_{n'm} = \begin{cases} -k_0G_j\displaystyle\int_{-L}^{0}\frac{x}{L}\sin(\mu_{n'}x)\,\mathrm{d}x, & m=0, \\ -k_0G_j\displaystyle\int_{-L}^{0}\frac{\sinh(\kappa^j_m x)}{\sinh(\kappa^j_m L)}\sin(\mu_{n'}x)\,\mathrm{d}x, & m=1,2,\ldots, \end{cases} \quad j=2,3,\ldots,N, \tag{85}$$

$$\overline{D}^{j,j+1}_{n'm} = \begin{cases} k_0G_j\displaystyle\int_{-L}^{0}\frac{x}{L}\sin(\mu_{n'}x)\,\mathrm{d}x, & m=0, \\ k_0G_j\cos(\kappa^{j+1}_m h_{j+1})\displaystyle\int_{-L}^{0}\frac{\sinh(\kappa^{j+1}_m x)}{\sinh(\kappa^{j+1}_m L)}\sin(\mu_{n'}x)\,\mathrm{d}x, & m=1,2,\ldots, \end{cases} \quad j=1,2,\ldots,N, \tag{86}$$

$$\overline{E}^{j,j-1}_{n'm'} = \frac{L}{2}G_j\beta^j_{n'}\delta_{n'm'}, \quad j=2,3,\ldots,N, \tag{87}$$

$$\overline{E}^{j,j}_{n'm'} = \begin{cases} \dfrac{L}{2}\alpha_{n'}\delta_{n'm'}, & j=1, \\ \dfrac{L}{2}\gamma^j_{n'}\delta_{n'm'}, & j=2,3,\ldots,N, \end{cases} \tag{88}$$

$$\overline{E}^{j,j+1}_{n'm'} = \frac{L}{2}G_j\beta^{j+1}_{n'}\delta_{n'm'}, \quad j=1,2,\ldots,N-1, \tag{89}$$

$$\overline{R}^{1}_{n} = -\delta_{n0}, \tag{90}$$

$$\overline{R}^{2}_{n} = \frac{-k_0\int_{-d_1}^{0} Z_0(z)f_{1,n}(z)\,\mathrm{d}z}{\lambda_n\coth(\lambda_n L)\int_{-d_1}^{0}\left(f_{1,n}(z)\right)^2\,\mathrm{d}z}, \tag{91}$$

$$\overline{R}^{1+j}_{n} = \begin{cases} \dfrac{-k_0L\int_{-d_j}^{-d_{j-1}} Z_0(z)\,\mathrm{d}z}{h_j}, & n=0, \\ \dfrac{-2k_0\int_{-d_j}^{-d_{j-1}} Z_0(z)f_{j,n}(z)\,\mathrm{d}z}{h_j\kappa^j_n\coth(\kappa^j_n L)}, & n=1,2,\ldots,M, \end{cases} \quad j=2,3,\ldots,N+1. \tag{92}$$

References

1. Yu X (2002) Functional performance of a submerged and essentially horizontal plate for offshore wave control: a review. Coast Eng J 44(02):127–147
2. Yu X, Chwang AT (1994) Water waves above submerged porous plate. J Eng Mech 120(6):1270–1282
3. Taylor G (1956) Fluid flow in regions bounded by porous surfaces. Proc R Soc Lond Ser A 234(1199):456–475
4. Chwang AT (1983) A porous-wavemaker theory. J Fluid Mech 132:395–406
5. Chwang AT, Wu J (1994) Wave scattering by submerged porous disk. J Eng Mech 120(12):2575–2587
6. Yu X (1995) Diffraction of water waves by porous breakwaters. J Waterw Port Coast Ocean Eng 121(6):275–282
7. Chwang AT, Chan AT (1998) Interaction between porous media and wave motion. Annu Rev Fluid Mech 30(1):53–84
8. Hsu HH, Wu YC (1998) Scattering of water wave by a submerged horizontal plate and a submerged permeable breakwater. Ocean Eng 26(4):325–341

9. Cho I, Kim M (2000) Interactions of horizontal porous flexible membrane with waves. J Waterw Port Coast Ocean Eng 126(5):245–253
10. Cho IH, Kim MH (2008) Wave absorbing system using inclined perforated plates. J Fluid Mech 608:1–20
11. Wu J, Wan Z, Fang Y (1998) Wave reflection by a vertical wall with a horizontal submerged porous plate. Ocean Eng 25(9):767–779
12. Yip T, Chwang AT (1998) Water wave control by submerged pitching porous plate. J Eng Mech 124(4):428–434
13. Yip T, Chwang AT (2000) Perforated wall breakwater with internal horizontal plate. J Eng Mech 126(5):533–538
14. Yip T, Sahoo T, Chwang AT (2002) Trapping of surface waves by porous and flexible structures. Wave Motion 35(1):41–54
15. Liu Y, Li YC, Teng B (2007) Wave interaction with a perforated wall breakwater with a submerged horizontal porous plate. Ocean Eng 34(17):2364–2373
16. Liu Y, Li YC, Teng B, Dong S (2008) Wave motion over a submerged breakwater with an upper horizontal porous plate and a lower horizontal solid plate. Ocean Eng 35(16):1588–1596
17. Zhao F, Bao W, Kinoshita T, Itakura H (2010) Interaction of waves and a porous cylinder with an inner horizontal porous plate. Appl Ocean Res 32(2):252–259
18. Behera H, Sahoo T (2015) Hydroelastic analysis of gravity wave interaction with submerged horizontal flexible porous plate. J Fluids Struct 54:643–660
19. Molin B (2011) Hydrodynamic modeling of perforated structures. Appl Ocean Res 33(1):1–11
20. An S, Faltinsen OM (2012) Linear free-surface effects on a horizontally submerged and perforated 2D thin plate in finite and infinite water depths. Appl Ocean Res 37:220–234
21. Neves MdG, Losada IJ, Losada MA (2000) Short-wave and wave group scattering by submerged porous plate. J Eng Mech 126(10):1048–1056
22. Liu Y, Li HJ, Li YC (2012) A new analytical solution for wave scattering by a submerged horizontal porous plate with finite thickness. Ocean Eng 42:83–92
23. Liu Y, Li YC (2011) An alternative analytical solution for water-wave motion over a submerged horizontal porous plate. J Eng Math 69(4):385–400
24. Cho I, Koh H, Kim J, Kim M (2013) Wave scattering by dual submerged horizontal porous plates. Ocean Eng 73:149–158
25. Liu Y, Li HJ (2014) Wave scattering by dual submerged horizontal porous plates: further results. Ocean Eng 81:158–163
26. Wang KH, Shen Q (1999) Wave motion over a group of submerged horizontal plates. Int J Eng Sci 37(6):703–715
27. Liu Y, Li YC, Teng B (2012) Interaction between obliquely incident waves and an infinite array of multi-chamber perforated caissons. J Eng Math 74(1):1–18
28. Linton CM, McIver P (2001) Handbook of mathematical techniques for wave/structure interactions. The Wiener-Hopf and related techniques, Chap 5. Chapman and Hall/CRC, Boca Raton
29. Yu X, Chwang AT (1994) Wave-induced oscillation in harbor with porous breakwaters. J Waterw Port Coast Ocean Eng 120(2):125–144
30. Isaacson M, Premasiri S, Yang G (1998) Wave interactions with vertical slotted barrier. J Waterw Port Coast Ocean Eng 124(3):118–126
31. Isaacson M, Baldwin J, Premasiri S, Yang G (1999) Wave interactions with double slotted barriers. Appl Ocean Res 21(2):81–91
32. Kellogg OD (1967) Foundations of potential theory. Sequences of harmonic functions. Springer, Berlin, pp 248–277
33. Lee JF (1995) On the heave radiation of a rectangular structure. Ocean Eng 22(1):19–34
34. Lan Y, Hsu T, Lai J, Chang C, Ting C (2011) Bragg scattering of waves propagating over a series of poro-elastic submerged breakwaters. Wave Motion 48(1):1–12
35. Evans DV, Peter MA (2009) Asymptotic reflection of linear water waves by submerged horizontal porous plates. J Eng Math 69(2):135–154
36. Mansard EP, Funke E (1980) The measurement of incident and reflected spectra using a least squares method. Coast Eng Proc 1(17)
37. Andria G, Savino M, Trotta A (1989) Windows and interpolation algorithms to improve electrical measurement accuracy. IEEE Trans Instrum Meas 38(4):856–863